# Numerical simulations of a full scale load test on a stone masonry arch bridge

J. Alfaiate
*Prof. Auxiliar, Instituto Superior Técnico, Lisbon, Portugal.*
*e-mail: alfaiate@civil.ist.utl.pt*

A. Gallardo
*Engenheiro Civil, Lisbon, Portugal.*
*e-mail: rop84393@mail.telepac.pt*

ABSTRACT: The reported information of a full scale load test to collapse on a single span arch bridge, carried out within the aim of a research program developed by the *Transport and Road Research Laboratory* in the UK, is taken as reference to assess the ability of a finite element model to reproduce the overall behaviour of stone masonry arch barrels. The adopted masonry modeling consists of a discrete approach, in which the joints are represented by initial zero thickness interface elements and the regularly cut to shape voussoirs are represented by continuum linear-elastic elements. The softening behaviour of the interfaces is modeled by a constitutive relation based upon the damage theory. The numerical results are compared to the data obtained from the experimental test. A comparison between the present numerical simulation and other simplified design procedures is also attempted.

## 1 INTRODUCTION

The work reported in the present paper was carried out with the aim of assessing the capability and adequacy of a numerical model to trace the behaviour of a masonry arch ring throughout an entire loading range, particulary giving attention to the early stages where a marked loss of stiffness seems to occur in consequance of initial crack openning. The information collected from a set of full scale load tests to failure undertook by the *Transport and Road Research Laboratory* (Hendry et al. 1986) provided an unvaluable and rare opportunity to validate the present method of structural analysis with real experimental data. The case studied was Bargower bridge, a semi-circular arch bridge with cut-to shape stone voussoirs. The backing of the arch springings was found to play a major role in the overhall structural response.

In the numerical model employed a discrete approach is considered, where masonry joints are idealized as zero-thickness interface elements and conventional continuum elements are used for the voussoirs. Backing contribution is taken as a boundary condition, by means off elastic supports acting horizontally.

Finally, the numerical results are discussed and compared with the experimental data and some conclusions are drawn.

## 2 MATERIAL MODELS AND NUMERICAL IMPLEMENTATION

In this Section the constitutive relationships adopted for masonry are presented. The stone blocks are assumed to behave as an isotropic linear elastic continuum. Fracture is allowed only at the masonry joints. Two different interface models are adopted, based on a discrete approach: i) a damage model and ii) a tension free model. In the damage model, a loading function is defined as:

$$f(w_n) = (w_n - \kappa_0) - \kappa, \tag{1}$$

where $w_n$ is the relative displacement measured between the opposite faces of the joint along the normal direction, $\kappa_0$ is the elastic normal relative displacement obtained at crack initiation and the internal variable $\kappa$ is a function of the maximum normal relative displacement reached, such that:

$$\kappa = \max[(w_n - \kappa_0) , 0], \qquad \kappa \geq 0, \qquad \dot{\kappa} \geq 0. \tag{2}$$

Before crack opening ($f < 0$, $\kappa = 0$), an elastic behaviour is adopted:

$$t_n = D_{nn}^{e} w_n, \qquad t_s = D_{ss}^{e} w_s \tag{3}$$

where $D_{nn}^{e}$ and $D_{ss}^{e}$ are elastic stiffness coefficients, $t_n$ and $t_s$ are the normal and shear traction components, respectively and $w_s$ is the sliding relative displacement. If $f = 0$, softening takes place as well as the evolution of damage ($\dot{\kappa} > 0$), where the dot denotes the time derivative, whereas if $f < 0$ and $\kappa > 0$, closing of the crack occurs and damage does not grow ($\dot{\kappa} > 0$). When damage increases ($\dot{\kappa} > 0$), an exponential softening law is adopted for the constitutive relation between the normal traction component $t_n$ and the normal relative displacement between crack faces $w_n$, such that

$$t_n = f_t \beta(\kappa), \quad \beta(\kappa) = \exp(-\frac{f_t}{G_F} k ), \tag{4}$$

where $f_t$ is the tensile strength of the joint, $G_F$ is the fracture energy adopted which is equal to the area below the softening curve shown in fig.1 and $\beta$ is a damage internal variable. Recalling equations (1), (3) and (4) the elastic normal relative displacement obtained at crack initiation, $\kappa_0$, is given by:

$$\kappa_0 = \frac{f_t}{D_{nn}} \quad . \tag{5}$$

Although the tensile principal stresses are practically aligned with the circumferential direction, small shear traction components can still develop at the interfaces. In order to enforce the shear traction component to decrease with increasing crack opening, the following relation is adopted for the shear traction component $t_s$ ($\dot{\kappa} > 0$):

$$t_s = t_s^{i} \beta(\kappa), \tag{6}$$

where $t_s^{i}$ is the elastic shear traction component obtained at crack initiation. Thus, under increased damage ($\dot{\kappa} > 0$), the incremental constitutive relation in matrix form is given by:

$$\begin{Bmatrix} \dot{t}_n \\ \dot{t}_s \end{Bmatrix} = \begin{bmatrix} -\frac{f_t^2}{G_F} ß & 0 \\ -t_s^{i} & 0 \end{bmatrix} \begin{Bmatrix} \dot{w}_n \\ \dot{w}_s \end{Bmatrix} \tag{7}$$

As a consequence, the shear traction component depends upon the normal relative displacement only, i.e., after crack initiation, the amount of sliding between crack faces does not influence the stress state anymore. If $w_n > 0$, the secant stiffness matrix is used for unloading and reloading, which is given by

$$D_{unloading} = \begin{bmatrix} -\frac{f_t ß}{k} & 0 \\ -\frac{t_s^{i} ß}{k} & 0 \end{bmatrix} \tag{8}$$

If a crack fully closes ($w_n \leq 0$), the elastic behaviour is recovered (see fig.1).

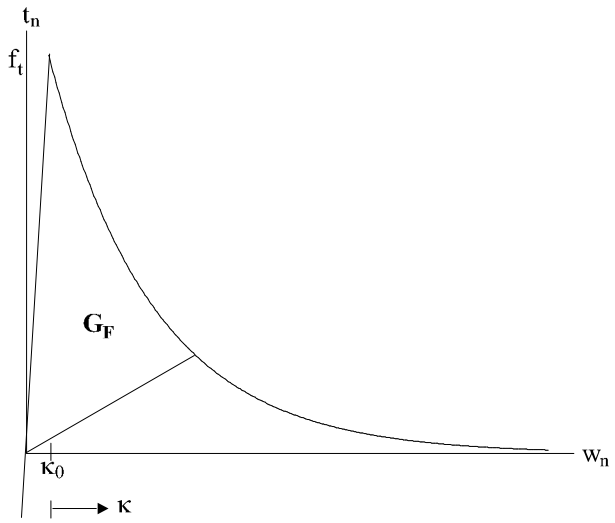


Figure 1. Exponential softening relationship adopted in the damage model

In the tension free model the joints open freely, without any tractions, whereas an elastic behaviour is adopted if $w_n \leq 0$. In this case, no tensile strength is adopted at the interfaces due to the ageing and consequent deterioration of the lime. The corresponding constitutive relation can be expressed in matrix form as:

$$\{t_n, t_s\} = [D_{nn}, 0, 0, D_{ss}]\{w_n, w_s\}, \tag{9}$$

where $D_{nn} = D_{nn}^{e}$ and $D_{ss} = D_{ss}^{e}$ if $w_n \leq 0$, or $D_{nn} = D_{ss} = 0$ otherwise.

The computational analysis of the masonry arch bridge is carried out by means of a finite element formulation, in which the units or blocks are represented by continuum plane stress elements while the lime joints are represented by interface elements, enabling to reproduce potential cracking arising at these joints. For the units, isoparametric 4-node elements are adopted whereas for the modelling of joints 4-node interface elements are used.

The use of non-linear stress-strain relationships requires an incremental iterative solution procedure, i.e., the loads are applied step by step and equilibrium iterations are carried out at each increment until equilibrium is reached within acceptable limits. For each step, the following algorithm is performed:

1. Evaluation of the tangent stiffness matrix of the structure, $\mathbf{K_t}$;
2. Solution of the system of equations $\mathbf{K_t}\Delta\mathbf{u} = \Delta\mathbf{F}$, where $\Delta\mathbf{u}$ is the vector of incremental displacements and $\Delta\mathbf{F}$ is the vector of incremental forces;
3. Determination of the internal forces $\Delta\mathbf{F_i}$. The Newton-Raphson method is used to obtain convergence. If equilibrium is satisfied, we proceed to step 4, otherwise a new iteration is performed; if no convergence is achieved after a given number of iterations, a smaller step is adopted and the process is repeated;
4. Evaluation of the total variables;
5. Return to 1.

In order to enhance the convergence of the iterative process, particularly when the load-displacement curve approaches a peak, the arc-length control is adopted. This technique has proved to be very useful for situations where the standard Newton-Raphson method often fails, such as in the case of snap-back behaviour that is known to occur frequently in masonry structures (Rots 1997, Almeida 1999). In the tests presented, a monotonic increase of the vertical displacement under the load is imposed. The incremental step size $\Delta\lambda$ is controlled such that the following equation is satisfied:

$$\frac{\Delta ?^2}{\Delta l_0^{\,2}} + \frac{|\Delta u|^2}{|\Delta u_0|^2} = 2.0, \tag{10}$$

where $\Delta\lambda_0$ is the initially prescribed incremental step size, D**u** is the vector of incremental displacements and D$\mathbf{u_0}$ is the vector of incremental displacements obtained in the first step.

## 3 RESULTS

### *3.1 Brief description of bridge and load test arrangement*

Bargower bridge arch ring had a semi-circular profile, built up of regularly cut to shape sandstone voussoirs. The bridge had a 16º skew angle and the arch ring courses were angled. Behind spandrel dressed stone facing walls, the presence of 1m thick inner side walls made up of rubble masonry was detected. Also, as revealed on bridge demolition, arch hauching consisted of crushed sandstone with clay traces, above wich spandrel filling was constructed with a silty gravelly sand. Principal dimensions of the tested bridge are listed in Table 1, being those adopted in finite element model presented herein.

Table 1 : Bargower principal dimensions

| | |
|---|---|
| Span (square) (m) | 10.00 |
| Span (skew) (m) | 10.36 |
| Rise at midspan (m) | 5.18 |
| Arch thickness (m) | 0.588 |
| Total width (m) | 8.68 |
| Fill depht at crown (m) | 1.20 |

The bridge was considered to be in moderate conservation state, presenting some defects wich were found to have no significant influence on the overhall structural capacity. Longitudinal cracks were observed, developing from springing to springing at least on one of the arch faces. Leaning outward parapets and spalling of individual stones due to frost were other of the observed defects.

Experimental data on sandstone specimens allowed to determine a compressive strength of 33.3MPa and a deformation modulus of 14.1MPa. The evaluated stone self weight was equal to 26.8kN/m$^3$ and, from available data, the fill self weight adopted in the present work is 20.0kN/m$^3$.

The test procedure consisted of the incremental application of load, by means of hidraulic jacks, to a concrete strip cast in the road surface across the full width of the bridge and located at a third span, where the minimum failure load was expected. The jack reactions against steel beams were supplied by ground anchors, set through the bridge deck. Although other relevant information was obtained and studied, in the present paper attention is mainly focused on the displacement of the arch ring, measured by means of precision surveying, taken at the third span points and at the crown of the arch. Such results will be presented in the following sections, altogether with the numerical simulations data.

### *3.2 Numerical solutions*

Several numerical tests were performed, yet sharing some basic assumptions of major relevance as certain aspects of stuctural behaviour are unknown. As usual, when a plane stress state is postulated, the contribution of the spandrel walls is ignored and, on the other hand, the absolute rigidity of the abutments is assumed. Geometric non-linearity effects are not included.

Remaining effects such as material non-linearity of the joints and the influence or arch backing in the arch response were analysed. Finite element mesh sensivity was initialy studied, leading to the conclusion that three bulk elements (as well as three interface elements) per voussoir depht, were adequate. As indicated by photographic records, the arch ring was subdivided into 53 equal wedge shaped masonry blocks, following the semi-circular profile above mentioned.

The material parameters adopted for the continuum elements were already described in section 3.1 and were directly taken from experimental data. In what concerns to joint filling properties there is no test information available, so the parameters for the interface elements had to be withdrawn from other masonry case studies (Rots 1997) and are listed in Table 2. These material parameters were used in accordance with the material model described in section 2.

Table 2 : Interface element properties

| | |
|---|---|
| Joint normal stiffness ($GN/m^3$) | 82 |
| Joint tangential stiffness ($GN/m^3$) | 36 |
| Tensile strenght of joint (MPa) | 1,0 |
| Mode I fracture energy ($kNm/m^2$) | 0.07 |

When considered, the contribution of arch backing was attained by means of linear spring supports, acting horizontally (Crisfield and Page 1990) and under compression only. Maximum compressive reaction was found to be always below the passive lateral pressure of the haunching material. The horizontal subgrade coefficient was assumed to vary linearly along the depth of the arch, within a value range of 1-3$MNm^{-2}$/m, which are considered good estimates for the material used in the Bargower bridge construction. Despite reasonably adjusted to the soil properties identified, the coefficient of subgrade reaction might have been considered even superior due to the constraints offered by the rock mass present bewind the bridge springing far from load line.

Loading was simulated by means of nodal forces at the extrados of the arch ring, according to the aproximated elastic degradation of a line load applied at the surface of the bridge deck.

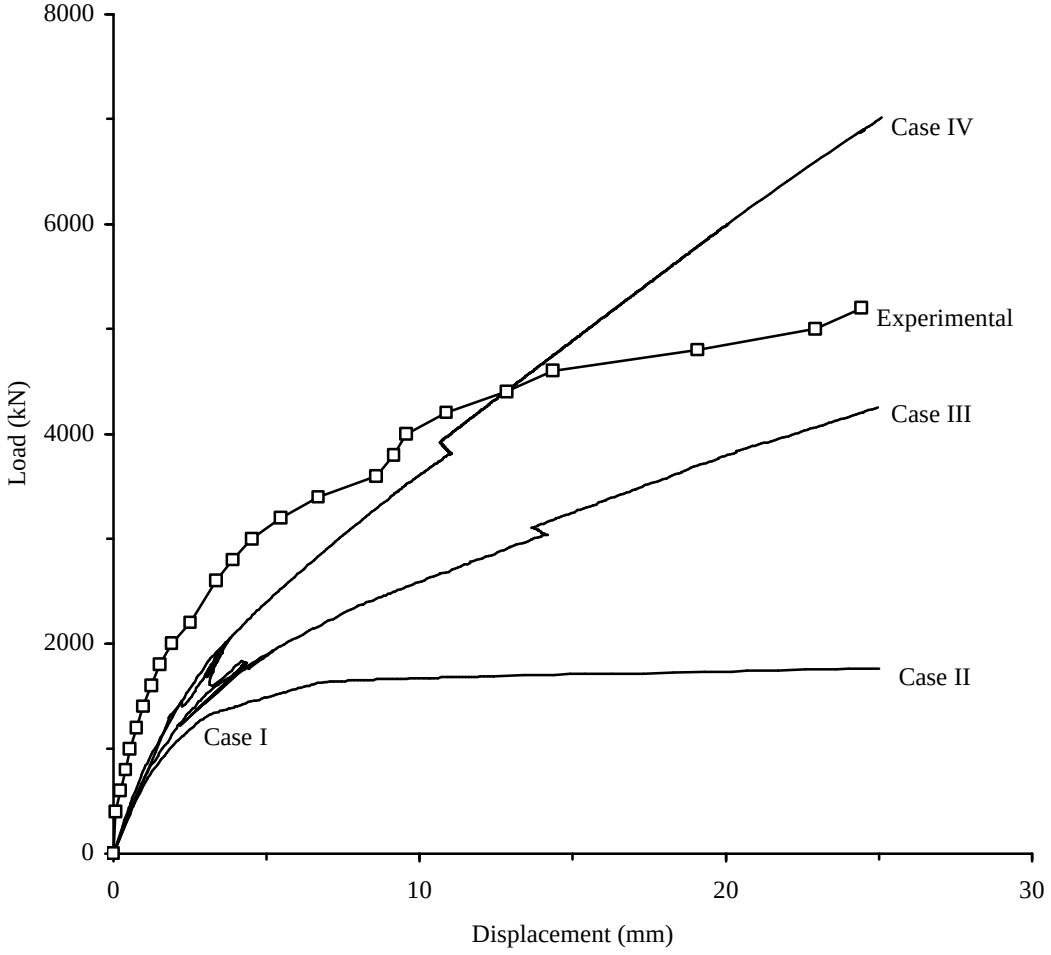


Figure 2 : Vertical displacement of arch soffit beneath load line

### *3.3 Numerical solutions and comparison with load test data*

Four simulations were undertaken. In the first one, hereby designated as Case I, the backing contribution was ignored and the interface Model I described in section 2 was adopted. The load-deflection relationship obtained beneath load line, in the vertical direction, is presented in Figure 2, altogether with other curves described forward in this section.

In the second simulation, designated as Case II, the tension free material model at interfaces, referred to in section 2, was adopted. Both the referred cases shared the same type of limitations in describing the real structural behaviour of Bargower Bridge. Figure 2 shows the load-deflection curve achieved in the current case and, as in the former case, the predicted relationship presents a less stiffer overall behaviour and points out for an ultimate load far below the one experimentally obtained load, circa 5600kN.

The deformed mesh represented in Figure 3 allows the identification of the collapse mechanism associated with the second simulation, revealing an realistic location of hinge formation at the outermost springing and an exaggerated sway movement towards the abutment. In fact, although a plateau was clearly achieved, an unlimited deformation is obtained, far behind from the limits of admissibility of linear geometric analysis and exhibiting a misleading idea of ductility that the real structure did not exhibit. Otherwise, it must be noted that, even at such large deformation stages, the compression stresses at interfaces were fairly below the compressive strength of the sandstone units, validating the assumption regarding the elastic model in compression adopted for the masonry units.

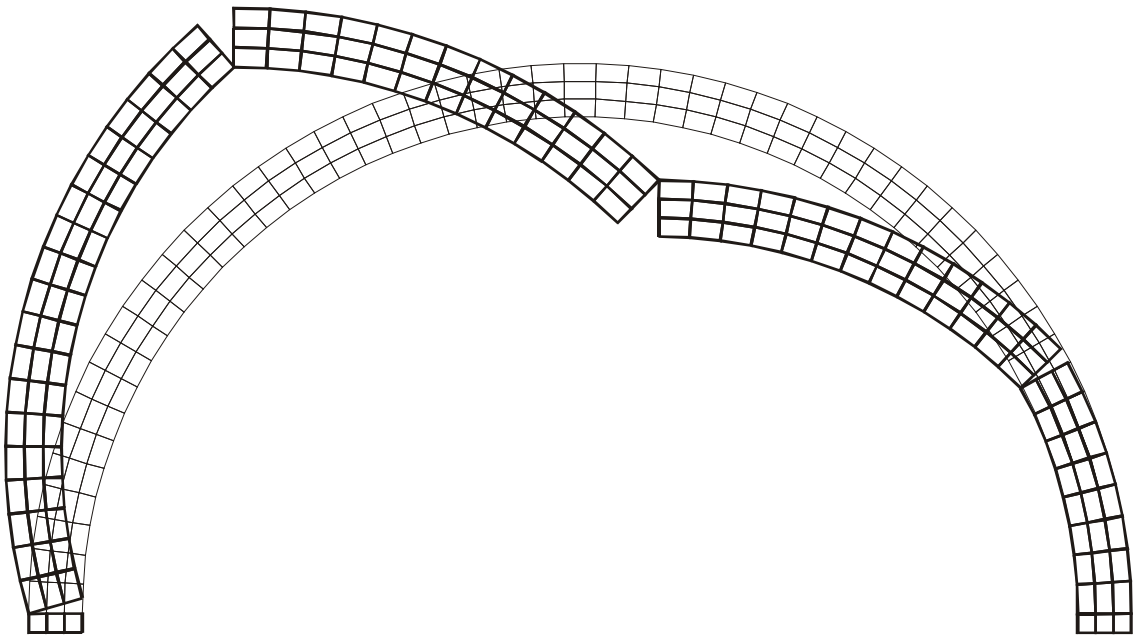

Figure 3 : Case II - Deformed mesh corresponding to a total load of 1770kN and a maximum displacement of 183mm beneath load line (displacements magnified 5 times)

In the third simulation, designated Case III, the interaction between the backing and the arch ring was attempted. Here, the fitting between numerical and experimental data improved qualitatively, showing the decisive contribution of arch haunching to the bridge behaviour. In fact, this results confirms the long known dependency of semi-circular arches from the sustaining effect of backing passive thrusts at springings (Crisfield and Page 1990).

According to the load-deflection curve beneath the load line, it is possible to devise a qualitatively similar non-linear behaviour as the one reflected by the real structure, which might be approximated by two linear responses. At the final deformation stage, the difference between experimental and numerical loads does not exceed 20% and the slope of the responses towards failure is similar.

Again, as in the above mentioned cases the finite element model used herein is unable to predict the collapse load, at least, until the threshold of compressive strength of masonry blocks is reached, which seems to happen within the range of geometric non-linearity. It is now pertinent to observe that the stiffness of the initial deformation stage obtained with the current numerical models is clearly smaller than the one observed in the real structure. In Figure 4 the predicted horizontal movement at crown voussoir is also compared with the experimental data, again showing the stiffer structural response of the real arch when compared with the numerical response.

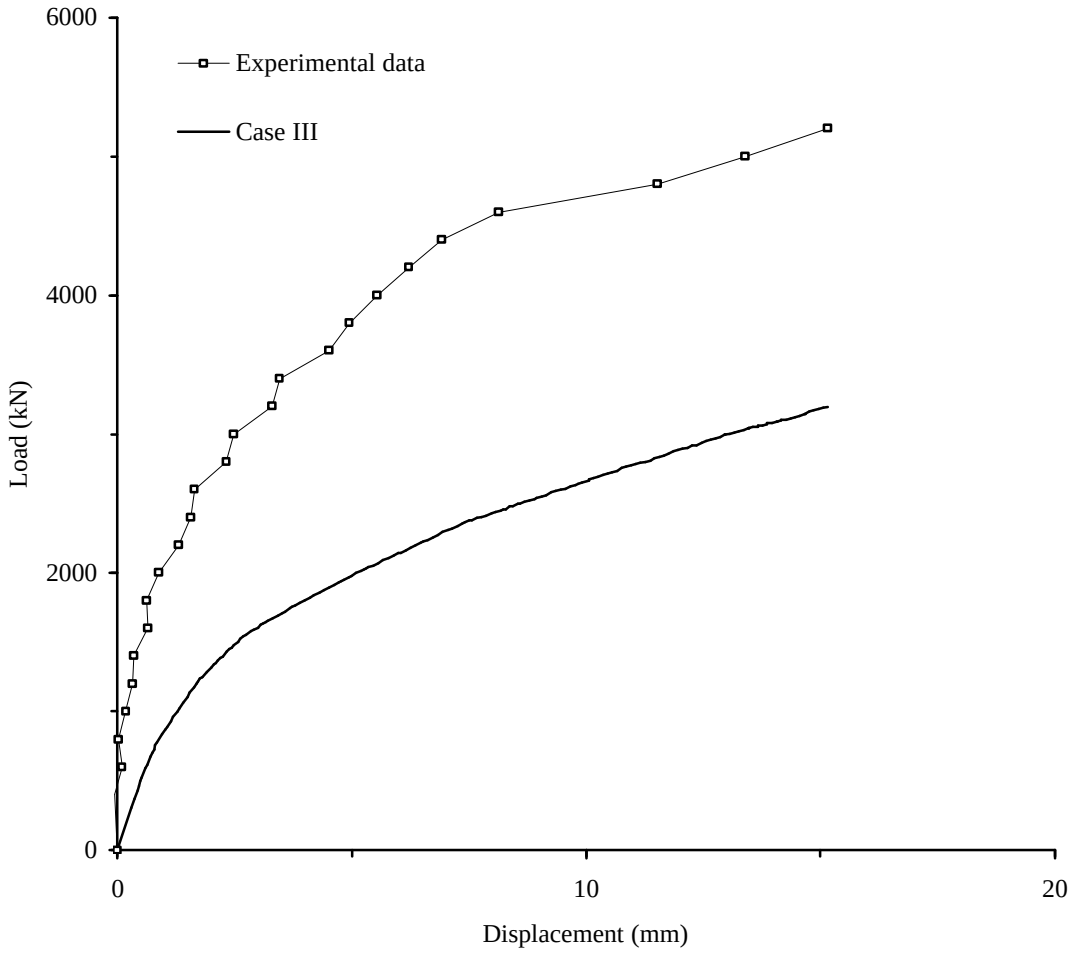


Figure 4 : Case III - Horizontal displacement of arch soffit at crown

As a consequence of taking into account the backing in the numerical model, the free outwards movement of the arch is now prevented, leading to a raise in the position of the remote hinge formation points as represented in Figure 5. In the present case, the formation and location of hinges seems to be in agreement with the assumptions adopted in mechanism models (Crisfield and Page 1990, Page 1995a), which led to values of collapse loads between 5750-9700kN, depending upon the adopted compressive strength of masonry.

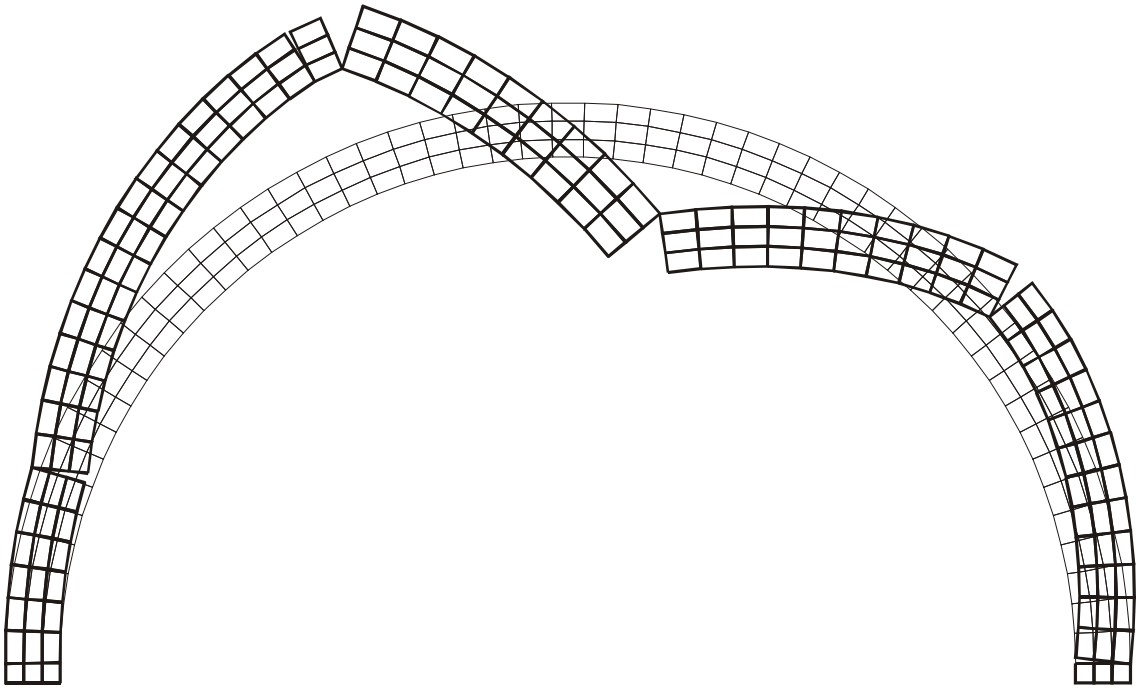

Figure 5 : Case III - Deformed mesh correspondent to a total load of 8150kN and a maximum displacement of 79mm beneath load line (displacements magnified 10 times)

Finally, in the fourth case studied, the backing subgrade coefficient was increased three times regarding the value adopted in the previous case. As a consequence, the global structural stiffness increased significantly at the later stage of the deformation curve, even above of the actual response obtained in the experimental test. Yet, despite the global rigidification of the arch, the indicial slope of the load-displacement relationship is still inferior to the experimentally exhibited. At the ultimate level of displacement considered (circa 25 mm), the load is now 25% greater than the collapse load of 5600kN.

## 4 CONCLUSIONS

The actual numerical model allows for the clear identification of the cracking pattern throughout the arch ring and as well as an easy detection of the collapse mechanism. Additional considerations can be made regarding the stiffness and the ultimate load numerically obtained. In particular:

i) the consideration of the haunching is found essential to reproduce more adequately the global behaviour of the structure. The experimentally found collapse mechanism can not be reproduced and the ultimate load is fairly underestimated unless the backing is taken into account on both lateral sides of the arch.
ii) However, the increase of the contribution of the backing may result in an ultimate stiffness and load which are clearly above the experimental ones.
iii) The tension free model adopted for the interfaces seems able to predict a smoother response of the structure than the damage model in which a non-zero tensile strength is adopted. In the latter case, strong snap-back responses are obtained which were not found experimentally.

In spite of i) and taking into account ii) it was not possible to approximate correctly the initial stiffness experimentally found. This is due to the fact that the correct knowledge of the material parameters is not possible, apart form other aspects of the structural behaviour which were not taken into account, such as the non-linear contribution of the haunching, the contribution of the spandrel walls mentioned above or the influence of the pavement. Furthermore, it was observed experimentally that the collapse occurs simultaneously with the splitting of some stone blocks under the load line, which might have happened due to weathering and ageing effects.

REFERENCES

Almeida, J.R. and Alfaiate, J., *The study of confined masonry walls submitted to imposed displacements and temperature effects*, Proceedings of the ECCM'99, European Conference on Computational Mechanics, Munich, Germany, (1999).

Crisfield, M.A. and Page, J. 1990. Assessment of the load carrying capacity of arch bridges. In A.M. Sowden (ed), *The maintenance of brick and stone masonry structures*, p. 81-113. E. & F.N. Spon.

Hendry, A.W., Davies, S.R., Royles, R., Ponniah, D.A., Forde, M.C. and Komeyli-Birjandi, F. 1986. *Test on masonry arch bridge at Bargower*. Contract. Rep. 26. Transport and Road Research Laboratory. Crowthorne, Berks.

Page, J. 1995. Load tests to collapse on masonry arch bridges. In C. Melbourne (ed), *Arch bridges*, p. 289-298. Thomas Telford, London.

Page, J. 1995. Load tests for assessment of in-service arch bridges. In C. Melbourne (ed), *Arch bridges*, p. 299-306. Thomas Telford, London.

*Structural masonry, an experimental/numerical basis for practical design rules*, Edited by J.G. Rots, A.A.Balkema, Rotterdam, (1997)